Transparent Nanoprobes in Integrated Plasmonic Circuits Based on Plasmonic Cloaking

Dimitrios C. Zografopoulos*
Consiglio Nazionale delle Ricerche, Istituto per la Microelettronica e Microsistemi, Via del fosso del cavaliere 100, 00133 Rome, Italy

Konstantinos P. Prokopidis
Department of Electrical and Computer Engineering, Aristotle University of Thessaloniki, Thessaloniki GR-54124, Greece

(Received 27 October 2014; revised manuscript received 28 November 2014; published 23 December 2014)

Cloaking of nanoscopic objects via the scattering-cancellation technique is theoretically demonstrated in integrated plasmonic circuits with deep subwavelength confinement in the infrared. By proper design of the cloaking shell, transparency of the cloaked objects can be achieved, even when these objects occupy the whole cross section of a metal-insulator-metal waveguide. The effects of material losses, possible implementations, and potential applications are discussed.

DOI: 10.1103/PhysRevApplied.2.064009

I. INTRODUCTION

A constantly growing amount of scientific research has been devoted in recent years to the field of metamaterials, a term coined to describe an expanding group of artificial materials, which are characterized by electromagnetic properties that cannot be encountered in their natural counterparts. Such properties, for instance engineerable permittivity and permeability ranging from negative to zero and positive values, enable unprecedented possibilities in the control of electromagnetic (EM) waves from microwave up to optical frequencies [1,2], indicative examples being subwavelength focusing and perfect lensing [3], or the cloaking of objects so that they are rendered invisible to surrounding radiation.

The latter, in particular, has been theoretically demonstrated following different approaches [4–7], among which the coordinate transformation [4,5] and the scattering cancellation technique (SCT) [8–15] have been identified as most promising. The first one relies on engineering the EM properties of the cloaked object's near environment in such a way that EM waves circumvent and do not interact with it, whereas the second is based on the minimization of the overall scattering efficiency of the structure by introducing a specially designed cloak whose scattered field cancels on average that of the hidden object. Since the SCT is not based on resonant phenomena, it has been proven more robust to variations from the optimal design in terms of geometry and target frequency [10–12]. Furthermore, contrary to cloaking based on transformation optics, the impinging EM wave *does* interact with the cloaked object, a property which paves the way for applications such as "invisible" sensors [16], receiver antennas [14], and noninvasive nanotips in near-field scanning optical microscope (SNOM) measurements [13].

Although the cloaking properties of subwavelength objects have been thus far studied mostly in the context of free-space applications, the enhancement of the measurement efficiency of a SNOM tip investigated in Ref. [13] indicates that the cloaking technique can be also applied in more particular geometries, where guided waves could also be involved. In this work, we extend the SCT to the field of densely integrated infrared plasmonic optical circuits with deep subwavelength confinement. It is demonstrated that cylindrical objects with plasmonic cloaking inside nanoscale metal-insulator-metal (MIM) plasmonic waveguides [17] exhibit minimal reflection even when these objects occupy the whole cross section of the light-wave propagation channel. The effect of material dispersion and losses is investigated, revealing some intrinsic limits of the approach for the case of realistic materials. Since such cloaked nanoscopic objects interact with propagating light without disturbing its flow, they could act as in-line distributed transparent nanoprobes, e.g., photodetectors, sensors, or quantum dot emitters, in integrated plasmonic architectures, thus providing the basis for new applications in nanophotonic communications, plasmonic sensing and/or nanofluidics.

II. CLOAKED NANOPROBES IN INTEGRATED PLASMONIC WAVEGUIDES

As a starting point, we consider the case of infinite cylindrical objects with a subwavelength radius a_c and relative permittivity ε_c cloaked by a concentric cylindrical shell characterized by a_s and ε_s, as shown in Fig. 1(a). Both core and shell materials are nonmagnetic ($\mu_s = \mu_c = 1$) and the excitation field is a transverse-electric

*Corresponding author.
dimitrios.zografopoulos@artov.imm.cnr.it

 © 2014 American Physical Society

(TE) polarized—with respect to the cylinder axis—normally impinging plane wave at the free-space wavelength $\lambda_0 = 1.5\ \mu$m. Following an analysis based on the derivation of the coefficients describing Mie scattering from concentric cylindrical objects, it has been demonstrated in Ref. [15] that the scattering cross section (SCS) of the cloaked particle in the long-wavelength limit can be minimized by matching the shell radius and permittivity according to

$$\frac{\alpha_s}{\alpha_c} = \sqrt[2n]{\frac{(\varepsilon_s - \varepsilon_c)(\varepsilon_s + 1)}{(\varepsilon_s - 1)(\varepsilon_s + \varepsilon_c)}}, \tag{1}$$

where n is the angular order. In order to investigate the scattering properties of this system we employ a full-wave finite-element solver [18], using the scattered-field formulation, for the geometry described in Fig. 1(a). The radius a_s is fixed at 100 nm and the core material has a relative permittivity $\varepsilon_c = 3$.

Figure 2 plots the SCS of the core-shell system as a function of ε_s and a_c, normalized to the reference SCS of a 100-nm cylinder of $\varepsilon_c = \varepsilon_s = 3$. Two regions of particular interest are revealed, which correspond to enhanced and suppressed values of SCS, respectively. It can be observed that the locus of the numerical solution corresponding to minimum SCS is very well predicted by Eq. (1), calculated for $n = 1$, and indicated as a dashed line in Fig. 2. This analysis demonstrates that the first-order ($n = 1$) solution provided by Eq. (1) adequately describes the conditions that lead to minimal scattering, and thus efficient cloaking of the core cylinder. The maximum scattering solutions in Fig. 2 are also expected in such systems [19], however, the investigation of their properties lies beyond the scope of this work.

As the next step, we consider the case where the ensemble of nanocylinders is placed inside an Ag-air-Ag plasmonic waveguide of width $d_{\rm wg}$, as depicted in Fig. 1(b). We investigate the limiting case where $d_{\rm wg} = 2a_s$, i.e., when the cloaked cylinder occupies the whole cross section of the waveguide. Although light in MIM waveguides is confined in a deep subwavelength scale, the profile of the fundamental propagating plasmonic mode is quasi-TEM as evidenced in the inset of Fig. 3(a), with the magnetic field pointing along the cylinder's axis. Owing to this similarity, the transmission-line theory, as well as various semianalytical techniques, are implemented as an efficient tool for the fast analysis of MIM plasmonic circuits [20–22]. Therefore, although light is confined and guided between the two metallic layers, the profile of the EM field resembles the plane-wave excitation in the case of the free-space nanocylinders of Fig. 2, thus posing the question of whether or not the same design can also be applied to cloak nanoparticles inside MIM plasmonic circuits.

We consider three cases of $d_{\rm wg}$ and let ε_c vary in the range from 1 to 13, which covers most dielectric materials, e.g., polymers, glasses, transparent oxides, and semiconductors. For each set of $(\varepsilon_c, d_{\rm wg})$ an optimal value of ε_s is retrieved via finite-element simulations, which maximizes transmittance through the MIM waveguide, the latter normalized to that of an empty waveguide of the same length. Figure 3(a) demonstrates that even under such conditions of extreme subwavelength light confinement, the closed-form solution of Eq. (1) provides an accurate estimate of the cloaking design parameters. In all three cases studied, the normalized transmittance is $\simeq$100%, irrespective of the permittivity of the cloaked material. This property is demonstrated in Fig. 3(b), in which the transmittance of the uncloaked core cylinders in the same geometry and the electric-field profiles calculated for the cloaked and noncloaked cylinder with $\varepsilon_c = 10$ and $d_{\rm wg} = 200$ nm are also plotted for comparison. In all calculations, silver is modeled as a dispersive Drude critical-points

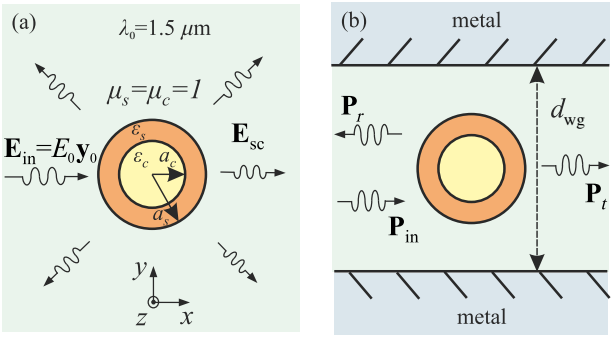

FIG. 1. Structural layout and parameter definition of a nonmagnetic cloaked nanocylinder at $\lambda_0 = 1.5\ \mu$m (a) for a TE-impinging plane wave in free space and (b) in a metal-insulator-metal plasmonic waveguide, excited by its fundamental mode.

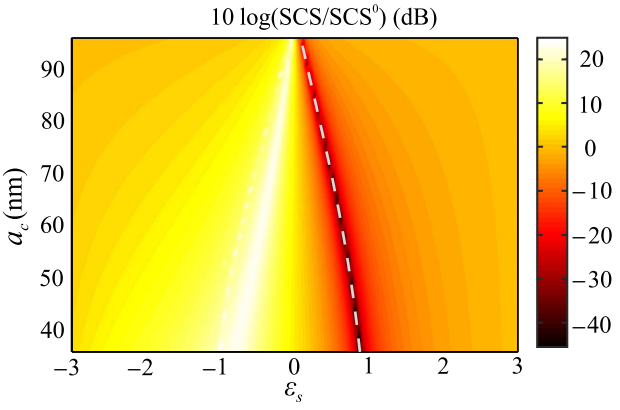

FIG. 2. Scattering cross section (SCS) of a nanocylinder with radius a_c and relative permittivity $\varepsilon_c = 3$ as a function of the cloaking shell permittivity ε_s for a fixed total radius $a_s = 100$ nm. Results are normalized to the SCS of a reference 100-nm nanocylinder with $\varepsilon_s = \varepsilon_c = 3$. The SCS minima that correspond to the solution of Eq. (1) are indicated by the dashed line.

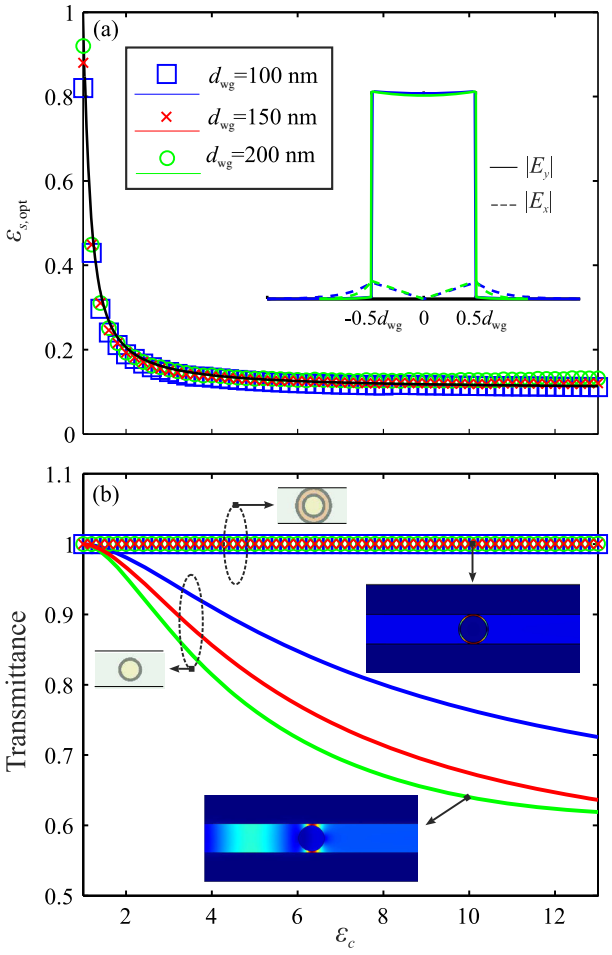

FIG. 3. (a) Numerically calculated optimal permittivity values of the plasmonic shell that minimizes the scattering of a nanocylinder with $a_c = 0.9a_s$ in an Ag-air-Ag waveguide of width $d_{wg} = 2a_s$, for different values of core permittivity ε_c. The continuous line is the solution given by Eq. (1). The inset shows the field profile of the fundamental mode's electric-field components. (b) Normalized transmittance of the waveguide for the cloaked and noncloaked nanocylinders, showing almost 100% transmittance for the cloaked case. The insets show the electric-field profiles for a nanocylinder with $\varepsilon_c = 10$ and $d_{wg} = 200$ nm in both cases, indicating zero reflectance when the cloaking shell is employed.

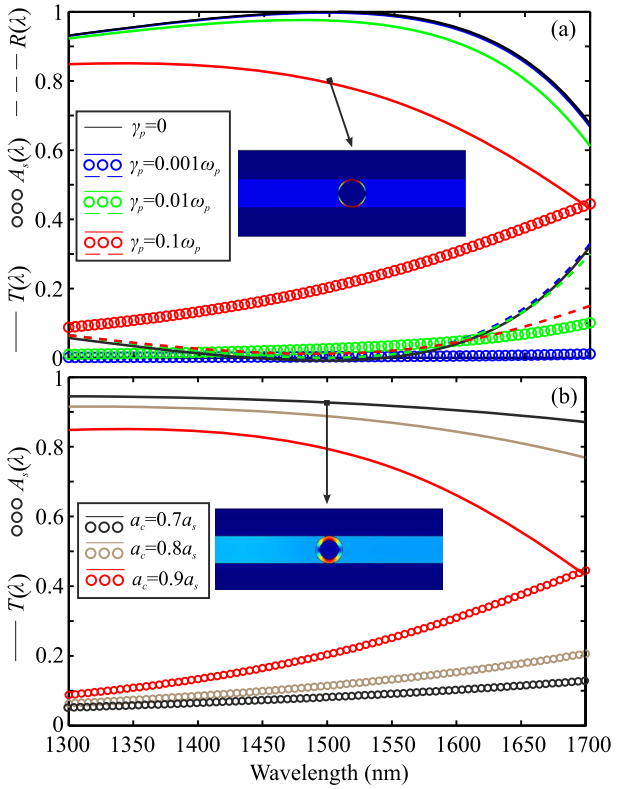

FIG. 4. (a) Broadband transmittance, reflectance, and absorption of an optimally cloaked cylinder of $a_c = 45$ nm and $\varepsilon_c = 10$ in an Ag-air-Ag plasmonic waveguide with $d_{wg} = 2a_s = 100$ nm, assuming a Drude model for the dispersion of the cloaking shell material and various levels of dumping losses. Time-domain propagation of a monochromatic sinusoidal wave through both a cloaked and a noncloaked waveguide is shown in the Supplemental Material for the lossless case [25]. (b) Lower absorption is possible by employing thicker cloaking shells for the same value of material loss $\gamma_p = 0.1\omega_p$. The insets show the corresponding electric-field profiles at 1.5 μm.

material, corresponding to $\varepsilon_{Ag} = -107.4 - 8.3j$ at 1.5 μm [23,24].

In order to study the broadband behavior of the optimally cloaked MIM nanocylinders, we describe the dispersive properties of the cloaking material via the Drude model $\varepsilon_s(\omega) = \varepsilon_\infty - \omega_p^2/(\omega^2 - j\omega\gamma_p)$, following the approach of [10,11]. We select the scenario characterized by $\varepsilon_c = 10$, $d_{wg} = 100$ nm, and $a_c/a_s = 0.9$, and fix the Drude model parameters as $\varepsilon_\infty = 1$, $\omega_p = 0.941\omega_0$, so that $\varepsilon_s(\lambda_0) = \varepsilon_{s,opt}(\lambda_0) = 0.114$, where $\omega_0 = 2\pi c_0/\lambda_0$ and c_0 is the speed of light *in vacuo*. The material losses are expressed via the collision frequency γ_p, which is allowed to vary from zero up to $0.1\omega_p$. Figure 4(a) shows the transmittance of the structure in the spectral window from 1300 to 1700 nm, for different values of γ_p. In the lossless case, transmittance stays close to 100% in for more than ± 50 nm with respect to the target wavelength λ_0. The exact extent of this high-transmittance spectral window depends on the particular material dispersion parameters, in this case ε_∞ and ω_p, as well as the eventual dispersive properties of the core material. For instance, semiconductors in the IR show appreciable dispersion, although the analysis in Fig. 2(a) demonstrates that for core materials with permittivity values in that range, the optimal value of the cloaking shell permittivity does not depend notably on ε_c. In any case, the results of Fig. 4(a) demonstrate that the cloaking property can be, in principle, broadband, a property that can be attributed to the nonresonant nature of the cloaking effect [10,11].

As the material losses are increased, part of the optical field energy is dumped in the plasmonic shell, resulting in decreased transmission. However, it is remarked that at the

central wavelength the reflectance is very low even when considerable amounts of losses are assumed. The inset of the electric-field profile in Fig. 4(a) reveals that the electric field is enhanced in the thin plasmonic shell ($a_c = 0.9a_s$), leading to absorption losses. As a possible way to reduce the absorption in the cloaking shell, Fig. 4(b) investigates the case where smaller core cylinders of the same material $\varepsilon_c = 10$ are covered by optimally designed cloaks with $2a_s = d_{\rm wg}$. The cloak is still modeled as a Drude material by adjusting ε_∞ so that the real part of $\varepsilon_s(\lambda_0)$ is equal to the optimal value for each value of a_c. It is demonstrated that thicker cloaks lead to lower absorbance for the same amount of material losses, fixed at $\gamma_p = 0.1\omega_p$. Reflectance is negligible at 1.5 μm and stays below 3% in the whole spectrum under study for $a_c = 0.7a_s$, indicating that although some energy is lost in the cloaking layer, the object does not perturb the flow of light in the plasmonic waveguide. It is pointed out that in this work we are considering the limiting case $d_{\rm wg} = 2a_s$, in which the plasmonic cloak is in direct contact with the silver-air interfaces of the MIM waveguide.

Up to this point, the geometry of the plasmonic circuit has been considered to be two dimensional, i.e., assuming nanocylinders of infinite length. In realistic designs, plasmonic slot waveguides (PSW) of finite height are typically patterned on top of a dielectric substrate, as demonstrated in the layout of Fig. 5(a). This configuration is experimentally demonstrated to allow for efficient coupling of the plasmonic circuit with dielectric nanowires compatible with the silicon photonics platform [26]. The mode profile of the fundamental mode is still TEM-like and is mostly confined in the slot region, although some leakage in the adjacent dielectric media occurs, as shown in Fig. 5(b). We have examined the lossless scenario studied in Fig. 4(a) and calculated the transmittance and reflectance of the slot waveguide, for a silica substrate of $\varepsilon_{\rm SiO_2} = 2.1$ and PSW height $h_{\rm wg} = 200$ nm. For these design parameters, the PSW achieves excellent shielding of the finite-height nanocylinder at the target wavelength λ_0, demonstrating that the proposed approach is valid also in the case of three-dimensional slot waveguides.

The same design procedure can be followed in cases where other spectral windows are targeted, e.g., in the visible or midinfrared. The Drude model assumed for the description of the cloaking shell dispersion is a valid approximation for the available choices of candidate materials for the realization of the proposed structures. In the visible, particularly the long-wavelength part of the spectrum, these can be noble metals or metal-dielectric composites that provide an overall metamaterial effect with engineerable permittivity values [27,28]. In the near- or midinfrared spectrum, extensive research is being carried out on low-loss plasmonic materials, mostly transparent conductive oxides (TCO), such as ITO, Al-doped or Ga-doped ZnO, or doped semiconductors, which are being

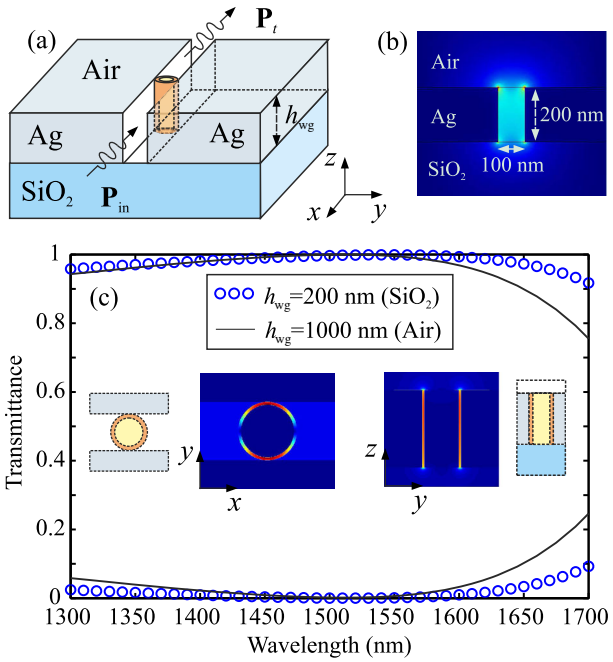

FIG. 5. (a) Schematic layout of a three-dimensional plasmonic slot waveguide on a silica substrate. (b) Electric-field profile of the fundamental mode of a 100-nm-wide and 200-nm-high PSW, calculated at 1.5 μm. (c) Cloaking performance of the three-dimensional PSW structure for the lossless shell case. A reference result calculated assuming air as the substrate material and $h_{\rm wg} =$ 1 μm is included, which tends to the results of the 2D MIM structure studied in Fig. 4(a). The inset shows the electric-field profile at 1.5 μm for two cross sections of the nanocylinder.

employed in the nanoengineering of artificial materials [29–33]. Among these, for instance, Al-doped ZnO shows the lowest overall losses and it can be engineered so that the cross-over wavelength is in the infrared. In general, doped TCOs are considered a suitable class of materials for devices relying on localized surface plasmon resonances, epsilon-near-zero, or metamaterial effects [34]. Other possibilities for the cloaking layer might include plasmonic satellite nanoparticles or multilayer structures as investigated in Refs. [35,36].

One of the most important properties of cloaking subwavelength objects by means of the SCT is that the electromagnetic field penetrates the hidden object, thus allowing for the interaction of the cloaked element with the external world is possible. This concept can be exploited in the realization of cloaked sensors or detectors and, by virtue of reciprocity, antennas, as extensively discussed in Refs. [13,14,16]. This can be the main potential field of applications envisaged for the proposed integrated cloaked nanoprobes. In particular, nanoscale photodetectors, e.g., semiconductors, quantum dots, or nanocrystals [37,38], have already been proposed for the direct reception of optical signals in integrated MIM circuitry [39–41]. In parallel, integrated sources are also being investigated for

plasmonic circuits, using quantum dots, semiconductor gain materials, or plasmon lasers [42–44]. Cloaking such nanosources or detectors might provide a platform to in- and out-couple information in MIM-based plasmonic circuits, without affecting the flow of light. These points of information exchange could be distributed inside the plasmonic network, allowing for in-line signal generation or detection.

The use of carrier-doped materials may also present an additional advantage, namely the possibility of dynamically tuning the doping level, and thus the plasmonic material's permittivity, by applying a control voltage across the MIM waveguide. In the infrared, TCOs are demonstrated to offer the potential for dynamic control of their permittivity values in nanometric crystals or layers of ITO, by controlling charge accumulation in ITO-dielectric interfaces in the presence of moderate electric fields [45–47]. The metallic layers, an essential part of MIM waveguides, could provide a ready selection for the control electrodes. In such a way, switching between the cloaked and noncloaked states of the nanoprobe can be targeted, in a dual approach compared to the tuning of plasmonic cloaks via external magnetic fields, as proposed in Ref. [48]. Finally, by inverting the principle of operation, the cloaking material could act as a sensing element, based on the large field enhancement and/or absorption in the cloaking layer, along the lines of doped-semiconductor plasmonic nanoantennas demonstrated as sensitive sensors in the midinfrared range [49,50].

III. CONCLUSIONS

In brief, we have demonstrated that by using the scattering-cancellation technique, transparent nanoprobes can be placed in highly integrated plasmonic circuits in the infrared. The minimization of their scattering cross section is manifested as minimal back reflection in the optical waveguide channel. The optical field is nonzero in the cloaked object, suggesting that it can be used as an in-line point for in- or out-coupling information, without affecting the flow of light in the circuit. The effect of material dispersion and losses has been discussed, as well as envisaged applications based on state-of-the-art materials and techniques.

[1] *Metamaterials: Physics and Engineering Explorations*, edited by N. Engheta and R. W. Ziolkowski (Wiley & Sons, New York, 2006).

[2] W. Cai and V. Shalaev, *Optical Metamaterials* (Springer, New York, 2010).

[3] J. B. Pendry, Negative refraction makes a perfect lens, Phys. Rev. Lett. **85**, 3966 (2000).

[4] J. B. Pendry, D. Schurig, and D. R. Smith, Controlling electromagnetic fields, Science **312**, 1780 (2006).

[5] W. Cai, U. K. Chettiar, A. V. Kildishev, and V. M. Shalaev, Optical cloaking with metamaterials, Nat. Photonics **1**, 224 (2007).

[6] N. A. P. Nicorovici, G. W. Milton, R. C. McPhedran, and L. C. Botten, Quasistatic cloaking of two-dimensional polarizable discrete systems by anomalous resonance, Opt. Express **15**, 6314 (2007).

[7] A. Alù and N. Engheta, Plasmonic and metamaterial cloaking: Physical mechanisms and potentials, J. Opt. A **10**, 093002 (2008).

[8] A. Alù and N. Engheta, Pairing an epsilon-negative slab with a mu-negative slab: Resonance, tunneling and transparency, IEEE Trans. Antennas Propag. **51**, 2558 (2003).

[9] A. Alù and N. Engheta, Achieving transparency with plasmonic and metamaterial coatings, Phys. Rev. E **72**, 016623 (2005).

[10] A. Alù and N. Engheta, Plasmonic materials in transparency and cloaking problems: Mechanism, robustness, and physical insights, Opt. Express **15**, 3318 (2007).

[11] A. Alù and N. Engheta, Dispersion characteristics of metamaterial cloaking structures, Electromagnetics **28**, 464 (2008).

[12] A. Alù and N. Engheta, Effects of size and frequency dispersion in plasmonic cloaking, Phys. Rev. E **78**, 045602(R) (2008).

[13] A. Alù and N. Engheta, Cloaked near-field scanning optical microscope tip for noninvasive near-field imaging, Phys. Rev. Lett. **105**, 263906 (2010).

[14] A. Alù and N. Engheta, Cloaking a receiving antenna or a sensor with plasmonic metamaterials, Metamaterials **4**, 153 (2010).

[15] A. Alù, D. Rainwater, and A. Kerkhoff, Plasmonic cloaking of cylinders: Finite length, oblique illumination and cross-polarization coupling, New J. Phys. **12**, 103028 (2010).

[16] A. Alù and N. Engheta, Cloaking a sensor, Phys. Rev. Lett. **102**, 233901 (2009).

[17] J. A. Dionne, L. A. Sweatlock, H. A. Atwater, and A. Polman, Plasmon slot waveguides: Towards chip-scale propagation with subwavelength-scale localization, Phys. Rev. B **73**, 035407 (2006).

[18] Commercial finite-element solver "COMSOL MULTIPHYSICS" Ver. 4.4, Comsol Inc., 2014.

[19] A. Alù and N. Engheta, Polarizabilities and effective parameters for collections of spherical nanoparticles formed by pairs of concentric double-negative, single-negative, and/or double-positive metamaterial layers, J. Appl. Phys. **97**, 094310 (2005).

[20] E. Feigenbaum and H. A. Atwater, Resonant guided wave networks, Phys. Rev. Lett. **104**, 147402 (2010).

[21] S. R. Mirnaziry, A. Setayesh, and M. S. Abrishamian, Design and analysis of plasmonic filters based on stubs, J. Opt. Soc. Am. B **28**, 1300 (2011).

[22] C. Lin, M. A. Swillam, and A. S. Helmy, Analytical model for metal-insulator-metal mesh waveguide architectures, J. Opt. Soc. Am. B **29**, 3157 (2012).

[23] K. P. Prokopidis and D. C. Zografopoulos, A unified FDTD/PML scheme based on critical points for accurate studies of plasmonic structures, J. Lightwave Technol. **31**, 2467 (2013).

[24] A. Vial, T. Laroche, M. Dridi, and L. Le Cunff, A new model of dispersion for metals leading to a more accurate

modeling of plasmonic structures using the FDTD method, Appl. Phys. A **103**, 849 (2011).

[25] See Supplemental Material at http://link.aps.org/supplemental/10.1103/PhysRevApplied.2.064009 for the time-domain propagation of a sinusoidal signal at $\lambda_0 = 1.5$ μm for $\varepsilon_c = 10$, $d_{\mathrm{wg}} = 100$ nm, and $a_c = 45$ nm, with and without the application of the plasmonic cloaking shell. Results are calculated via a dispersive formulation of the finite-difference time-domain method, adapted for the study of plasmonic structures [23]. Silver is modeled as a Drude critical points material [24] and the plasmonic shell as a lossless ($\gamma_p = 0$) Drude medium, with parameters as described in the text. The y component of the electric field is plotted.

[26] B. Lau, M. A. Swillam, and A. S. Helmy, Hybrid orthogonal junctions: Wideband plasmonic slot-silicon waveguide couplers, Opt. Express **18**, 27048 (2010).

[27] A. Monti, F. Bilotti, and A. Toscano, Optical cloaking of cylindrical objects by using covers made of core-shell nanoparticles, Opt. Lett. **36**, 4479 (2011).

[28] A. Ciattoni, R. Marinelli, C. Rizza, and E. Palange, $|\epsilon|$-Near-zero materials in the near-infrared, Appl. Phys. B **110**, 23 (2013).

[29] G. V. Naik, J. Liu, A. V. Kildishev, V. M. Shalaev, and A. Boltasseva, Demonstration of Al:ZnO as a plasmonic component for near-infrared metamaterials, Proc. Natl. Acad. Sci. U.S.A. **109**, 8834 (2012).

[30] H. Kim, M. Osofsky, S. M. Prokes, Glembocki, and A. Piqué, Optimization of Al-doped ZnO films for low loss plasmonic materials at telecommunication wavelengths, Appl. Phys. Lett. **102**, 171103 (2013).

[31] J. Kim, G. V. Naik, N. K. Emani, U. Guler, and A. Boltasseva, Plasmonic resonances in nanostructured transparent conducting oxide films, IEEE J. Sel. Top. Quantum Electron. **19**, 4601907 (2013).

[32] J. Kim, G. V. Naik, A. V. Gavrilenko, K. Dondapati, V. I. Gavrilenko, S. M. Prokes, O. J. Glembocki, V. M. Shalaev, and A. Boltasseva, Optical properties of gallium-doped zinc oxide—A low-loss plasmonic material: First-principles theory and experiment, Phys. Rev. X **3**, 041037 (2013).

[33] H. Caglayan, S.-H. Hong, B. Edwards, C. R. Kagan, and N. Engheta, Near-infrared metatronic nanocircuits by design, Phys. Rev. Lett. **111**, 073904 (2013).

[34] G. V. Naik, V. M. Shalaev, and A. Boltasseva, Alternative plasmonic materials: Beyond gold and silver, Adv. Mater. **25**, 3264 (2013).

[35] M. G. Silveirinha, A. Alù, and N. Engheta, Infrared and optical invisibility cloak with plasmonic implants based on scattering cancellation, Phys. Rev. B **78**, 075107 (2008).

[36] M. G. Silveirinha, A. Alù, and N. Engheta, Cloaking mechanism with antiphase plasmonic satellites, Phys. Rev. B **78**, 205109 (2008).

[37] P. Martyniuk and A. Rogalski, Quantum-dot infrared photodetectors: Status and outlook, Prog. Quantum Electron. **32**, 89 (2008).

[38] X. Liu and M. T. Swihart, Heavily-doped colloidal semiconductor and metal oxide nanocrystals: an emerging new class of plasmonic nanomaterials, Chem. Soc. Rev. **43**, 3908 (2014).

[39] D.-S. Ly-Gagnon, K. C. Balram, J. C. White, P. Wahl, M. L. Brongersma, and D. A. B. Miller, Routing and photodetection in subwavelength plasmonic slot waveguides, Nanophotonics **1**, 9 (2012).

[40] M. Gu, P. Bai, and E.-P. Li, Enhancing the reception of propagating surface plasmons using a nanoantenna, IEEE Photonics Technol. Lett. **22**, 245 (2010).

[41] P. Neutens, P. V. Dorpe, I. De Vlaminck, L. Legae, and G. Borghs, Electrical detection of confined gap plasmons in metal-insulator-metal waveguides, Nat. Photonics **3**, 283 (2009).

[42] V. Sorger, N. Pholchai, E. Cubukcu, R. F. Oulton, P. Kolchin, C. Borschel, M. Gnauck, C. Ronning, and X. Zhiang, Strongly enhanced molecular fluorescence inside a nanoscale waveguide gap, Nano Lett. **11**, 4907 (2011).

[43] V. J. Sorger, R. F. Oulton, R.-M. Ma, and X. Zhiang, Toward integrated plasmonic circuits, MRS Bull. **37**, 728 (2012).

[44] Q. Li, H. Wei, and H. Xu, Resolving single plasmons generated by multiquantum-emitters on a silver nanowire, Nano Lett. **14**, 3358 (2014).

[45] G. Garcia, R. Buonsanti, E. L. Runnerstrom, R. J. Mendelsberg, A. Llordes, A. Anders, T. J. Richardson, and D. J. Milliron, Dynamically modulating the surface plasmon resonance of doped semiconductor nanocrystals, Nano Lett. **11**, 4415 (2011).

[46] E. Feigenbaum, K. Diest, and H. A. Atwater, Unity-order index change in transparent conducting oxides at visible frequencies, Nano Lett. **10**, 2111 (2010).

[47] Z. Lu, W. Zhao, and K. Shi, Ultracompact electroabsorption modulators based on tunable epsilon-near-zero-slot waveguides, IEEE Photon. J. **4**, 735 (2012).

[48] W. J. M. Kort-Kamp, F. S. S. Rosa, F. A. Pinheiro, and C. Farina, Tuning plasmonic cloaks with an external magnetic field, Phys. Rev. Lett. **111**, 215504 (2013).

[49] J. N. Anker, W. P. Hall, O. Lyandres, N. C. Shah, J. Zhao, and R. P. Van Duyne, Biosensing with plasmonic nanosensors, Nat. Mater. **7**, 442 (2008).

[50] S. Law, L. Yu, A. Rosenberg, and D. Wasserman, All-semiconductor plasmonic nanoantennas for infrared sensing, Nano Lett. **13**, 4569 (2013).